

**Wall thickness measurement using resonant phenomena of circumferential Lamb
waves generated by plural transducer elements located evenly on girth**

Hideo Nishino*, Kodai Iwata, and Masashi Ishikawa

Institute of Technology and Science, Tokushima University, Tokushima 770-8506,
Japan

E-mail: hidero.nishino@tokushima-u.ac.jp

Abstract

We present a novel method of measuring the pipe wall thickness using the resonance of the circumferential (C-) Lamb wave generated by a piezoelectric ring-shaped sensor (PS). The PS is a special device for an axially propagating torsional wave; however, the C-Lamb waves are generated simultaneously as spurious signals owing to the structure of the PS. Particularly under resonant conditions, the C-Lamb waves are dominantly generated, distorting the axially propagating wave. In this method, these troublesome spurious signals are used effectively for the measurement of the wall thickness under the PS location that is a dead zone of the PS itself. The method can compensate for its drawback, namely, the dead zone problem, without using additional instruments. In this study, the mechanisms of the generation and resonance of the C-Lamb waves were first explained. Secondly, the principle of the wall thickness estimation utilizing the resonance of the C-Lamb waves was proposed. Finally, experimental verifications were carried out. The estimated wall thicknesses agreed very well (maximum 1.5% error) with those measured by a micrometer caliper under suitable resonant conditions.

1. Introduction

Guided wave [1-13] inspection is one of the efficient and rapid screening techniques for various types of piping. The mathematical basics and fundamental features about the guided wave have been summarized well in some textbooks [6-8]. Basically, it does not give quantitative morphologies of defects; however, a quantitative evaluation of defect sizing has been investigated and reported [12-15]. Both the dry-coupled piezoelectric ring-shaped sensor (PS) [3] and the magnetostrictive sensor (MS) [9] are de facto standard devices for generating and detecting the guided waves propagating along the axial direction of piping. The PS consists of plural transducer elements located along the girth at regular intervals. These transducer elements vibrate transversely in the axial direction for the torsional mode guided waves [normally the $T(0,1)$ fundamental torsional mode]. Owing to the structure of the PS, in addition to the axially propagating torsional mode guided waves, the circumferential (C-) Lamb waves [6,7, 16-21] are also generated as spurious signals at the same time. Particularly under the resonant conditions determined by material parameters (bulk wave velocities and pipe dimensions), the C-Lamb waves are dominantly generated as spurious signals that distort the axially propagating torsional mode waves.

In this study, this troublesome phenomenon is used not for the axially propagating torsional mode guided waves but for the measurement of the wall thickness. The proposed method can inspect a region at the PS location where the axially propagating torsional mode waves cannot be inspected because of the dead zone. This feature is useful for actual industrial applications because no additional instrument is

needed to narrow the dead zone. Particularly in both the differential monitoring [13] and permanently installed sensor methods [14, 15], the present method is very useful because the PS is installed permanently at one axial location and the dead zone is fixed. Preliminary investigations of the present method have already been reported [22, 23]. Detailed investigations were carried out herein. The resonant phenomena of the circumferential shear horizontal (C-SH) wave [24, 25] [the other type of the circumferential guided wave] that converted from the T(0,1) mode themselves have been observed experimentally at axially elongated notches [26-28]. It has been confirmed that the reflection coefficients of the notches have been larger with the resonant conditions than those without the resonant conditions. The fatigue evaluation of the solid bar has also been carried out [29, 30] using the resonant phenomenon of the C-SH wave.

In this study, the resonant mechanism of the C-Lamb wave generated by the plural transducer elements located evenly on the girth is first described. A mathematical description shows the mechanism of constructing the standing wave generated by the plural transducer elements under specific conditions. Secondly, the principle of the wall thickness estimation by measuring the resonant frequency is explained on the basis of the dispersion relations (angular wavenumber versus frequency) of the C-Lamb wave. Finally, experimental verifications are carried out with 50A aluminum pipes having uniform wall thicknesses.

2. Resonant phenomena of C-Lamb wave

As described in Sect. 1, the PS consists of plural transducer elements located evenly on the girth. To generate the torsional guided waves including the fundamental $T(0,1)$ mode, the transducer elements vibrate along the circumferential directions. Figure 1 shows a schematic illustration of a pipe, one of the transducer elements, and the propagation paths of both axial torsional guided waves and the C-Lamb waves. One of the important things is that circumferential vibration generates not only axial torsional guided waves but also the C-Lamb waves. It can be understood intuitively that resonance occurs when the angular wavenumber (AWN) takes any natural number. Here, the AWN is the dimensionless real value that is defined as the number of wavelengths within the girth [16-20]. Figures 2(a) - 2(d) illustrate cross-sectional views of the resonant standing waves in the girth for four AWNs 1, 2, 4, and 8, respectively. Also depicted in Fig. 2 are the locations of all the eight transducer elements on the outer surface of the pipe. The eight transducer elements located evenly on the girth were used in the following experimental verifications. The arrows of the clockwise and counterclockwise directions in Fig. 2 indicate mutually asymmetric vibration phases. Under the vibration condition of AWN 8 shown in Fig. 2(d), all the transducer elements vibrate in the same phase. In this case, resonance occurs when the wavelength takes $1/8$ of the girth. Under the vibration condition of AWN 4 shown in Fig. 2(c), the vibration phase is set alternately in each transducer. In this case, resonance occurs when the wavelength takes $1/4$ of the girth.

To investigate quantitatively the resonant phenomena with the eight transducer elements, a simple mathematical model has been introduced. Here, the

phenomenon is based on the findings that the wave packets generated at the eight transmitter points are detected at a single receiving point. Each transmitter generates two wave packets, namely, the clockwise- and counterclockwise-propagating wave packets. As a result, sixteen wave packets are generated by the eight transmitters and are intermingled in the same circumferential orbit. The following mathematical model describes the accumulated amplitude of the sixteen wave packets at a single receiving point. If resonance occurs, the amplitude at the receiving point increases. Because a relatively large number of tone burst cycles is utilized in the method, it can be considered nearly as a monochromatic wave. According to the above assumption, the dispersion relation of the C-Lamb wave was neglected in the mathematical model. Actually, 13- and 25-cycles tone burst signals were used in the following experimental verifications.

In the mathematical model, the receiving point has been assumed to be located at position ① and possible transmitting points have been assumed to be located at all the eight circumferential positions shown in Fig. 2. In the above assumption, the amplitude observed at the receiving point can be obtained simply by accumulating all the waves traveling along both the clockwise and counterclockwise directions from the eight transducer elements. Therefore, the amplitude A is described as

$$A = \left| \sum_{k=1}^8 \sum_{n \in S} \left(\exp\{i\pi[(k-1)/4 + 2n]p\} + \exp\{-i\pi[(k-1)/4 + 2n]p\} \right) \right|, \quad (1)$$

$$S = \{n | 0 \leq l \leq [N/p - (k-1)/8]\}$$

where p , k , n , and N are the AWN of the C-Lamb wave, the identification number of the

transducer elements, the number of overlaps of the C-Lamb wave itself at the receiving point, and the number of tone burst cycles, respectively. The first and second terms on the right-hand side of Eq. (1) correspond to the waves propagating along the counterclockwise and clockwise directions, respectively. Equation (1) can be described as a real number notation in

$$A = 2 \left(\sum_{k \in R_1} \sum_{n \in S} \cos \{ \pi [(k-1)/4 + 2n] p \} - \sum_{k \in R_2} \sum_{n \in S} \cos \{ \pi [(k-1)/4 + 2n] p \} \right), \quad (2)$$

where R_1 and R_2 are the sets of identification numbers of transducer elements being vibrated in the same and inverse vibration phases, respectively. R_1 and R_2 regarding the four resonant conditions shown in Fig. 2 are as follows:

(1) As for the vibration condition of AWN 1 [Fig. 2(a)], transducer elements ⑧, ①, and ② are driven inversely with elements ④, ⑤, and ⑥; thus, R_1 and R_2 are

$$R_1 = \{k | 8, 1, 2\}, \quad R_2 = \{k | 4, 5, 6\}. \quad (3)$$

(2) As for the vibration condition of AWN 2 [Fig. 2(b)], transducer elements ① and ⑤ are driven inversely with elements ③ and ⑦; thus, R_1 and R_2 are

$$R_1 = \{k | 1, 5\}, \quad R_2 = \{k | 3, 7\}. \quad (4)$$

(3) As for the vibration condition of AWN 4 [Fig. 2(c)], transducer elements ①, ③, ⑤, and ⑦ are driven inversely with elements ②, ④, ⑥, and ⑧; thus, R_1 and R_2 are

$$R_1 = \{k | 1, 3, 5, 7\}, \quad R_2 = \{k | 2, 4, 6, 8\}. \quad (5)$$

(4) As for the vibration condition of AWN 8 [Fig. 2(d)], all the transducer elements are driven simultaneously in the same vibration phase; thus, R_1 and R_2 are

$$R_1 = \{k | 1, 2, 3, 4, 5, 6, 7, 8\}, \quad R_2 = \emptyset. \quad (6)$$

Figures 3(a) - 3(d) show the accumulated amplitudes (tone burst cycle $N = 25$) as a function of the AWN of the C-Lamb wave for the vibration conditions of AWNs 1, 2, 4, and 8, respectively. It was confirmed clearly that resonance occurred when the AWN of the C-Lamb wave was identical to each vibration condition. Several harmonic peaks could also be observed, as shown in Fig. 3. These results coincide with the intuitive speculation described above. As shown in Fig. 3, it was also confirmed that a sharper peak was observed at a lower AWN under all the four vibration conditions. The reason for these phenomena is that the number of overlaps, n , at a low AWN is larger than that at a high AWN.

3. Principle of the wall thickness estimation

Figure 4 shows the theoretical dispersion relations [16, 17, 19] of the C-Lamb wave propagating circumferentially in 60.5-mm-outer-diameter and 3.9- and 5.5-mm-thick aluminum ($c_l = 6400$ m/s and $c_t = 3160$ m/s) pipes. The lowest two modes (the CL_1 and CL_2 modes) are depicted. The CL_1 and CL_2 modes respectively indicate the modes that are similar to the A_0 - and S_0 -mode Lamb waves propagating in the plate. An important thing is that Fig. 4 shows the resonant frequencies obtained when the AWN takes natural numbers, that is, the standing waves are generated under those conditions. Since the dispersion relation changes with the wall thickness, its resonant frequency also changes with the wall thickness. This means that the wall thickness can be estimated by measuring the resonant frequency. This is considered the principle of the method. Particularly in the CL_2 mode at AWN 8, accurate estimations are anticipated

because the change in resonant frequency with the unit thickness is relatively large.

4. Experimental procedure

Figure 5 shows the experimental setup. The eight transmitter elements were located evenly on the girth and the receiver element was set 30 mm away from one of the transmitter elements along the axial direction, as shown in Fig. 5. This configuration of the transducer elements was determined by the structure of the dry-coupled piezoelectric ring-shaped sensor [31] that was used normally for the axial torsional guided waves. Each transducer element consists of PZT and its resonant frequency is around 2 MHz that is much higher than the frequency range of 20-150 kHz for guided wave inspection. Conversely, it has a flat frequency characteristic in the 20-150 kHz range. Two aluminum pipes were prepared for experimental verification. Both the dimensions and bulk wave velocities of the two specimen pipes are shown in Table I. The nominal pipe diameter of the two specimen pipes is the same at 60.5 mm and the nominal wall thicknesses of the two specimen pipes are 3.9 and 5.5 mm. The vibration conditions of the transmitter elements were set for AWNs 1, 2, 4, and 8, respectively (Fig. 2). 13- and 25-cycle tone burst signals were used as signal sources. The initial and final five cycles of tone burst signals were tapered up and down, respectively, with a cosine window function to avoid the generation of spurious high-frequency components. The 25-cycle tone burst signal is shown in Fig. 6.

5. Results and discussion

5.1 Time domain signals

Typical time domain signals without and with the resonance of the C-Lamb wave are shown in Figs. 7(a) and 7(b), respectively. These signals were observed with the 3.9-mm-nominal-thick pipe (Table I) under the vibration condition of AWN 8. The wave packets observed at a propagation time of around 0.0 ms are the T(0,1) mode torsional guided waves received immediately at the receiver element next to the transmitter elements. Resonance was observed at 65 kHz, but it was not observed at 55 kHz. Resonance can be observed as a signal decaying with the long time duration as shown in Fig. 7(b). Figures 8(a) and 8(b) respectively show the frequency variations (40 - 90 kHz) of the time domain signals generated by 13- and 25-cycle tone burst signals for the two specimen pipes under the vibration condition of AWN 8. It was confirmed that resonances occurred at around 65 and 85 kHz for the 3.9- and 5.5-mm-nominal-thick pipes, respectively. The resonant frequency did not change with the number of tone burst cycles. The time durations of the resonant signals for the 25-cycle tone burst signal were longer than those for the 13-cycle tone burst signal and the frequency ranges of the resonances for the 25-cycle tone burst signal were narrower than those for the 13-cycle tone burst signal. These phenomena mean that the resonances for the 25-cycle tone burst signal were stronger than those for the 13-cycle tone burst signal. Figures 9(a) and 9(b) show the frequency variations (100 - 150 kHz) of the time domain signals observed under the vibration condition of AWN 4 for 13- and 25-cycle tone burst signals, respectively. It was clearly confirmed that the resonant phenomena were almost the same as those observed under the vibration condition of

AWN 8 as shown in Figs. 8(a) and 8(b).

5.2 Resonant characteristics

The amplitudes at the propagation times of 20 - 40 cycle periods were determined from the frequency variation of the time domain signals. Figures 10(a) and 10(b) show the amplitude distributions at the propagation period of 20 - 40 cycles as a function of frequency for the 13- and 25-cycle signals, respectively. The 3.9-mm-nominal-thick specimen was used and the vibration condition of AWN 8 was employed. In all the cases shown in Figs. 10(a) and 10(b), almost the same center frequency could be observed (Table II). The quality factors [defined as center frequency/FWHM] regarding the 13 and 25 cycle tone burst signals were 8.96 ± 0.31 and 3.92 ± 0.07 , respectively. Figures 11(a) and 11(b) show again the amplitude distributions at the propagation period of 20 cycles for the 13- and 25-cycle tone burst signals, respectively. The solid lines in Figs. 11(a) and 11(b) indicate the results of calculation using Eq. (2). Here, the number of tone burst cycles, N , in the calculations was set to 8 and 20 in spite of the actual experimental cycles of 13 and 25. For the cosine window function applied to the tone burst signals in the experiments shown in Fig. 6, the actual time duration of the windowed burst signal was set to the time at which the amplitude took the half maximum of itself. It was confirmed that the calculation results agreed well with the experimental results.

5.3 Center frequencies of resonances and wall thickness estimations

As shown in Fig. 10, resonance occurred around finite frequency ranges. To estimate the wall thickness, the center frequency of resonance must be determined. The

center frequency at each cycle period was first determined by Gaussian curve fitting to the corresponding amplitude distribution (Fig. 10). Finally, the center frequency of resonance was determined by averaging the individual center frequencies for the propagation period of the five cycles. The experimental and theoretical resonant frequencies are summarized in Table II. The resonant frequencies as a function of wall thickness under the vibration conditions of AWNs 1, 2, 4, and 8 are shown in Figs. 12(a) - 12(d), respectively. Circles and triangles (both open and closed marks) in Fig. 12 indicate the experimental results obtained using 13- and 25-cycle tone burst signals, respectively. Solid and dashed lines in Fig. 12 show the theoretical calculations using the bulk wave velocities (Table I) for the two specimen pipes, respectively. The theoretical calculations between the two specimen pipes are slightly different owing to the minute difference in bulk wave velocities shown in Table I. The open marks should be compared with the dashed lines and the closed marks should be compared with the solid lines. All the frequency measurements agreed well (maximum 0.9% error) with the theoretical calculations.

Table III shows the estimated wall thicknesses under four vibration conditions. The experimental results were in good agreement with the wall thicknesses measured by the micrometer caliper. Particularly under the vibration condition of AWN 8, the estimations agreed excellently (maximum 1.5% error) with the measured wall thicknesses. This is because the change in resonant frequency with the unit thickness is relatively large compared with those observed under the other three vibration conditions.

In this section, validations of the present method using the pipes with uniform wall thicknesses are shown. Preliminary investigations [32] have already shown that the average wall thicknesses of pipes with uneven wall thicknesses could be measured by the present method. Future work will verify the efficiency of the present method using pipes with uneven wall thicknesses. It was shown clearly that the present method can inspect the region under the PS and can reduce the dead zone.

6. Conclusions

A novel method for measuring the pipe wall thickness using the resonance of the circumferential (C-) Lamb wave was proposed and evaluated. This method utilizes the dry-coupled piezoelectric ring-shaped sensor (PS) used normally for the transductions of the axially torsional guided waves, which can inspect the region under the PS and can reduce the dead zone of the PS without any additional instrument. It is very useful as one of the supplemental functions for an actual guided wave inspection system. In this paper, the mechanism of generating the resonances of the C-Lamb waves utilizing the PS at the specific frequencies is first presented. It was confirmed that the mathematical model agreed well with the resonant characteristics observed in the experiments. The accuracy of wall thickness estimation being realized by measuring the resonant frequency was evaluated under various resonant conditions. The experimental resonant frequencies coincided excellently with theoretical ones within 0.9% error. The accuracies of the wall thickness estimations using the pipes with uniform wall thicknesses were within 1.5% compared with those measured with the micrometer

caliper under the appropriate condition [vibration condition of AWN 8]. Future work will verify the efficiency of the present method using pipes with uneven wall thicknesses.

Acknowledgment

This work was supported by a Grant-in-Aid for Scientific Research (No. 25420041) in 2013-2015 from the Japan Society for the Promotion of Science.

Reference

- [1] D. C. Gazis: *J. Acoust. Soc. Am.* **31** (1959) 568.
- [2] A. H. Fitch: *J. Acoust. Soc. Am.* **35** (1963) 706.
- [3] D. N. Alleyne and P. Cawley: *J. Nondestr. Eval.* **15** (1996) 11.
- [4] D. N. Alleyne and P. Cawley: *Mater. Eval.* **55** (1997) 504.
- [5] M. J. S. Lowe, D. N. Alleyne, and P. Cawley: *Ultrasonics* **36** (1998) 147.
- [6] J. L. Rose: *Ultrasonic Waves in Solid Media* (Cambridge University Press, Cambridge, U.K., 1990).
- [7] J. L. Rose: *Ultrasonic Guided Waves in Solid Media* (Cambridge University Press, Cambridge, U.K., 2014).
- [8] D. Royer and E. Dieulesaint: *Elastic Waves in Solids I, Free and guided propagation* (Springer, Berlin, 2000).
- [9] H. Kwun and K. A. Bertels: *Ultrasonics* **36** (1998) 171.
- [10] H. Nishino, S. Takashina, F. Uchida, M. Takemoto, and K. Ono: *Jpn. J. Appl. Phys.* **40** (2001) 364.
- [11] T. Yamamoto, T. Furukawa, and H. Nishino: *Mater. Trans.* **57** (2016) 397.
- [12] H. Nishino: *Mater. Trans.* **56** (2015) 120.
- [13] H. Nishino, S. Masuda, Y. Mizobuchi, T. Asano, and K. Yoshida: *Jpn. J. Appl. Phys.* **49** (2010) 116602.
- [14] A. Galvagni and P. Cawley: in *Review of Progress in Quantitative Nondestructive Evaluation*, ed. D. O. Thomson and D. E. Chimenti (Plenum, New York, 2011) Vol. 31, p. 1591.

- [15] A. Galvagni and P. Cawley: in *Review of Progress in Quantitative Nondestructive Evaluation*, ed. D. O. Thomson and D. E. Chimenti (Plenum, New York, 2012) Vol. 32, p. 159.
- [16] I. A. Viktorov: *Rayleigh and Lamb Waves Physical Theory and Applications* (Plenum, New York, 1967) Chap. II, Sect. 10, p. 113.
- [17] G. Liu and J. Qu: *J. Appl. Mech.* **65** (1998) 424.
- [18] W. Luo, J. L. Rose, J. K. Van Velsor, M. Avioli, and J. Spanner: *AIP Conf. Proc.* **820** (2006) 165.
- [19] H. Nishino, R. Yokoyama, H. Kondo, and K. Yoshida: *Jpn. J. Appl. Phys.* **46** (2007) 4568.
- [20] H. Nishino, R. Yokoyama, K. Ogura, H. Kondo, and K. Yoshida: *Jpn. J. Appl. Phys.* **47** (2008) 3885.
- [21] H. Nagamizo, K. Kawashima, and J. Miyauchi: *Proc. Pressure Vessel and Piping*, 2003, p. 7.
- [22] H. Nishino, T. Kataoka, K. Morita, and K. Yoshida: *Proc. Ultrasonic Electronics*, 2011, p. 347.
- [23] H. Nishino and K. Morita: in *Review of Progress in Quantitative Nondestructive Evaluation*, ed. D. O. Thomson and D. E. Chimenti (Plenum, New York, 2013) Vol. 33, p. 246.
- [24] X. Zhao and J. L. Rose: *J. Acoust. Soc. Am.* **115** (2004) 1912.
- [25] H. Nishino and K. Yoshida: *Acoust. Sci. Technol.* **27** (2006) 389.
- [26] Z. Liu, C. He, B. Wu, X. Wang and S. Yang: *Ultrasonics* **44** (2006) e1135.

- [27] H. Kwun, S. Y. Kim, H. Matsumoto and S. Vinogradov: in *Review of Progress in Quantitative Nondestructive Evaluation*, eds. D. O. Thompson and D. E. Chimenti (American Institute of Physics, New York, 2008) Vol. 27, p. 193.
- [28] M. Ratssepp, S. Fletcher, and M. J. S. Lowe: *J. Acoust. Soc. Am.* **127** (2010) 730-740.
- [29] M. Hirao and H. Ogi: *Ultrasonics* **35** (1997) 413.
- [30] H. Ogi, M. Hirao, and K. Minoura: *J. Appl. Phys.* **81** (1997) 3677.
- [31] H. Nishino, T. Tanaka, S. Katashina, and K. Yoshida: *Jpn. J. Appl. Phys.* **50** (2011) 046601.
- [32] K. Iwata, K. Morita and H. Nishino: *Proc. Mechanical Engineering Congr.*, 2014, J0420201 [in Japanese].

Captions

Fig. 1. Schematic illustration of the torsional guided and circumferential Lamb waves. Both are generated by a shear transducer element on the surface of the pipe wall.

Fig. 2. Four standing waves depicted along with the pipe cross sections and the eight transducer elements: (a) $AWN = 1$, (b) $AWN = 2$, (c) $AWN = 4$, and (d) $AWN = 8$, where the AWN is defined as the number of wavelengths within the girth. The clockwise and counterclockwise arrows in each illustration indicate the mutually asymmetric vibration phases of the input signals for the preferential generation of resonances.

Fig. 3. Calculated amplitudes as a function of the AWN of the circumferential Lamb wave for four different vibration conditions depicted in Fig. 2: (a) $AWN = 1$, (b) $AWN = 2$, (c) $AWN = 4$, and (d) $AWN = 8$. The maximum peak in each graph is obtained when the AWN of the Lamb wave is equal to the corresponding vibration condition of the AWN .

Fig. 4. Theoretical dispersion relations of the circumferential Lamb wave ($v_t = 3160$ m/s, $v_l = 6400$ m/s, and outer diameter = 60.5 mm). This graph shows the relationship between the resonant frequency and the AWN only if the AWN takes any integers. Namely, the resonant frequencies are taken at all integers of the AWN .

Fig. 5. Experimental apparatus of the Al pipe, the eight transmitter elements, and the single receiver element. The pipe dimensions are shown in Table I.

Fig. 6. 25-cycle tone burst signal. The initial and last five cycles were tapered up and down, respectively, with quarter period cosine window functions to avoid harmonic generations.

Fig. 7. Time domain signals observed at (a) 55 and (b) 65 kHz. Resonance was observed as a signal decaying with long time duration.

Fig. 8. Frequency variations (lower 40 kHz – upper 90 kHz) of time domain signals generated by (a) 13- and (b) 25-cycle tone burst signals for pipes of 3.9 and 5.5 mm nominal thicknesses under vibration condition of AWN 8. The resonances could be found at around 65 and 85 kHz at nominal thicknesses of 3.9 and 5.5 mm, respectively.

Fig. 9. Frequency variations (lower 100 kHz – upper 150 kHz) of the time domain signals generated by (a) 13- and (b) 25-cycle tone burst signals for pipes of 3.9 and 5.5 mm nominal thicknesses under vibration condition of AWN 4.

Fig. 10. Amplitude distributions as a function of frequency for (a) 13- and (b) 25-cycle tone burst signals. Despite the difference between the tone burst cycles, the center frequency indicates almost the same value. It was confirmed clearly that the frequency

regions of the resonances for 25-cycle tone burst signal were narrower than those for 13-cycle tone burst signals.

Fig. 11. Theoretical and experimental resonant characteristics for (a) 13- and (b) 25-cycle tone burst signals.

Fig. 12. Resonant frequency versus wall thickness for four vibration conditions: (a) $AWN = 1$, (b) $AWN = 2$, (c) $AWN = 4$, and (d) $AWN = 8$. The thick and dotted lines indicate the theoretical relations that are calculated using the material parameters shown in Table I. The open and closed marks (both circles and triangles) show the experimental results of the 3.9- and 5.5-mm-nominal-thick pipes, respectively.

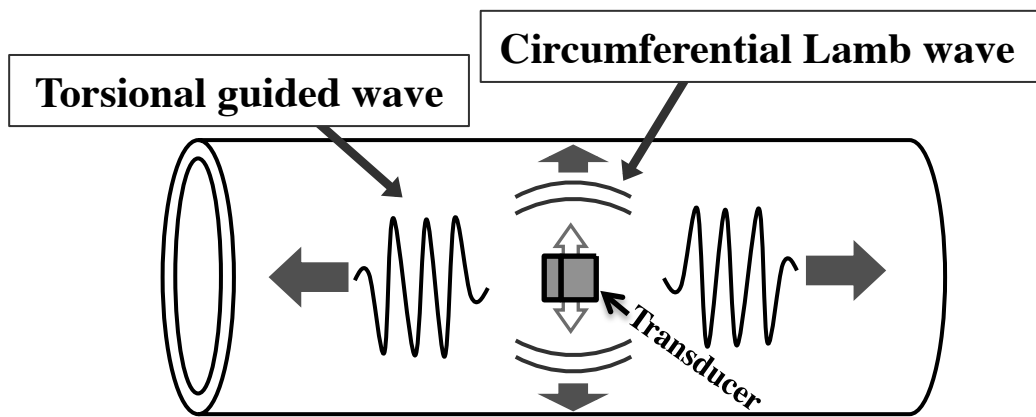


Figure 1 Nishino et al

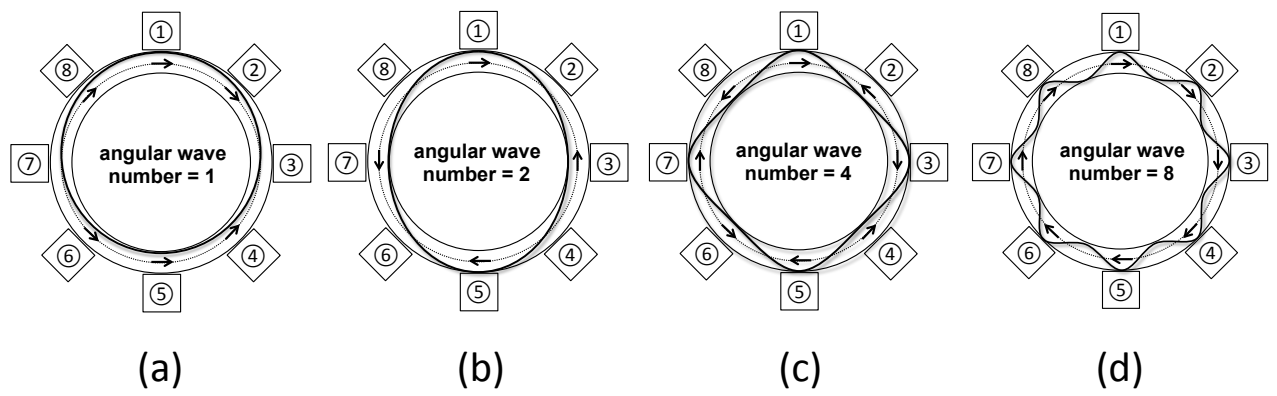
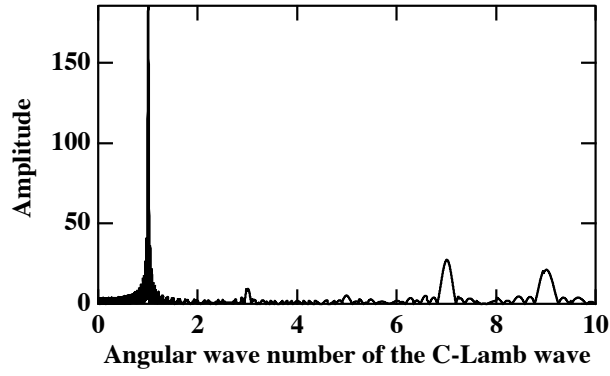
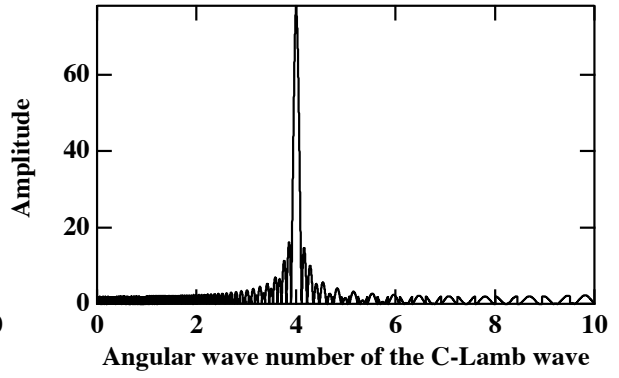


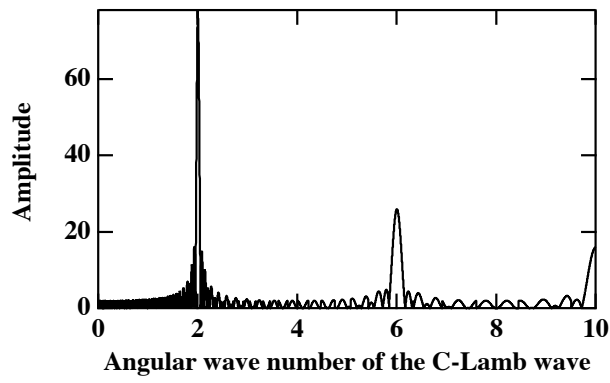
Figure 2 Nishino et al



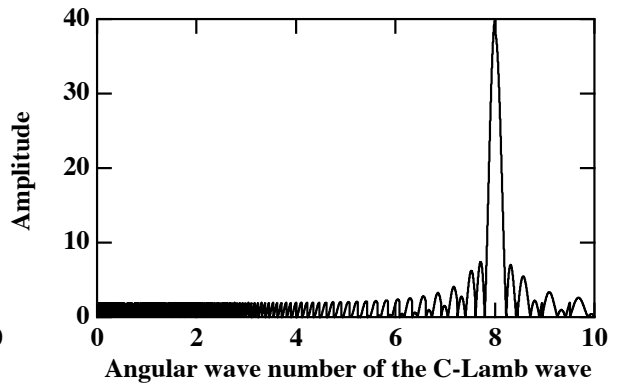
(a)



(b)



(c)



(d)

Figure 3 Nishino et al

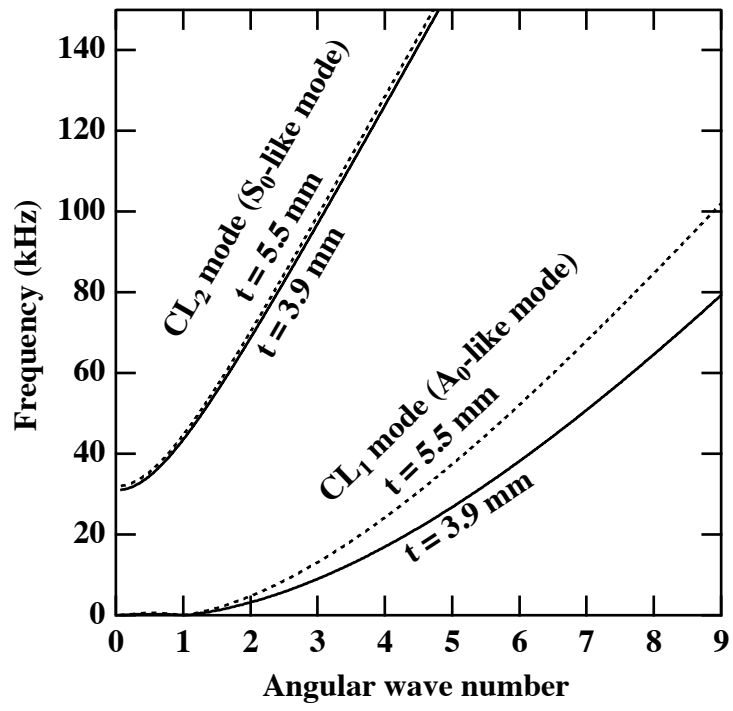


Figure 4 Nishino et al

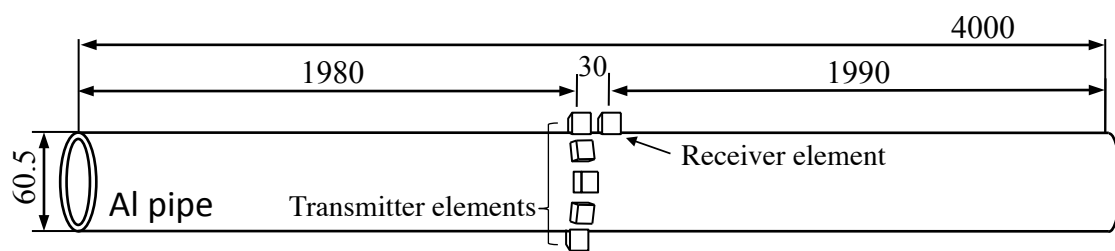


Figure 5 Nishino et al

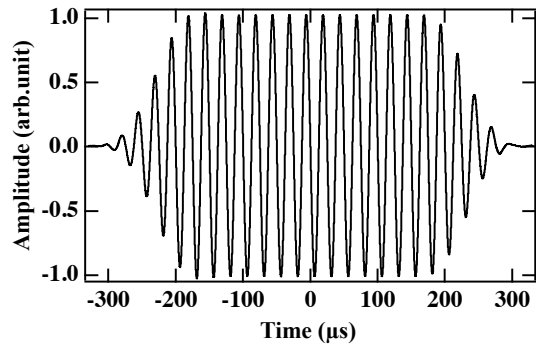
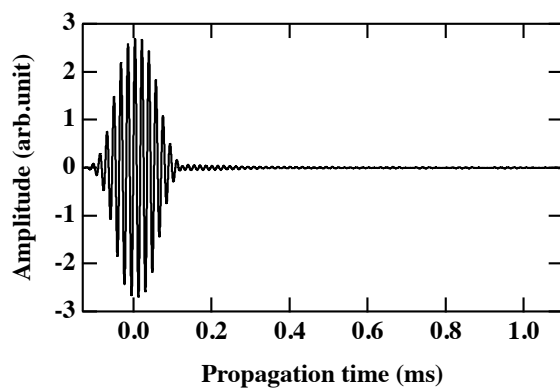
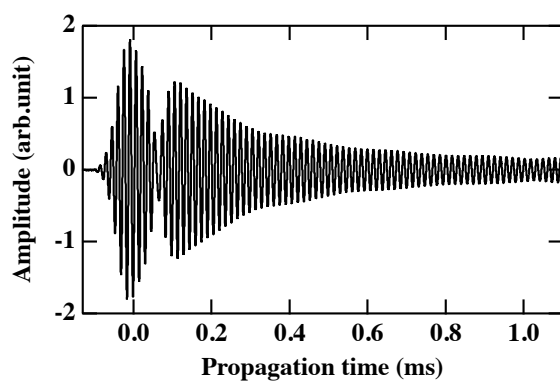


Figure 6 Nishino et al

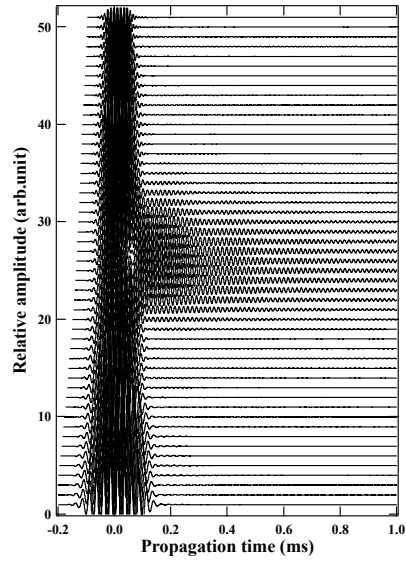


(a)

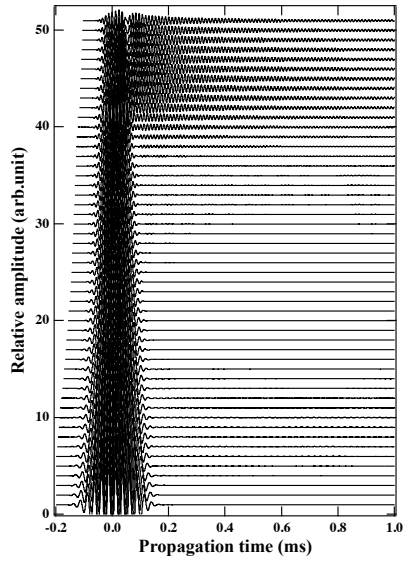


(b)

Figure 7 Nishino et al

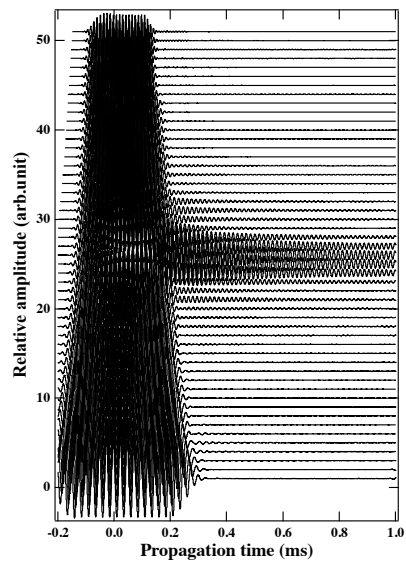


Wall thickness 3.9 mm

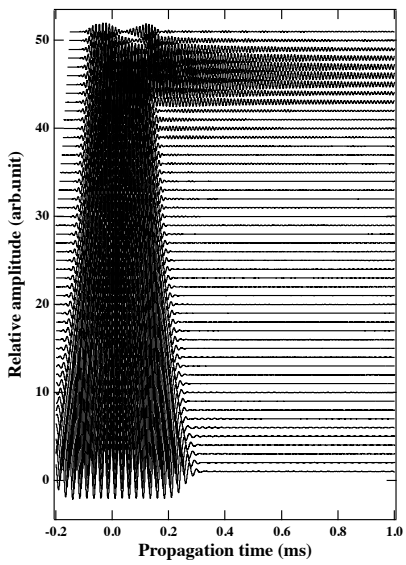


Wall thickness 5.5mm

(a)



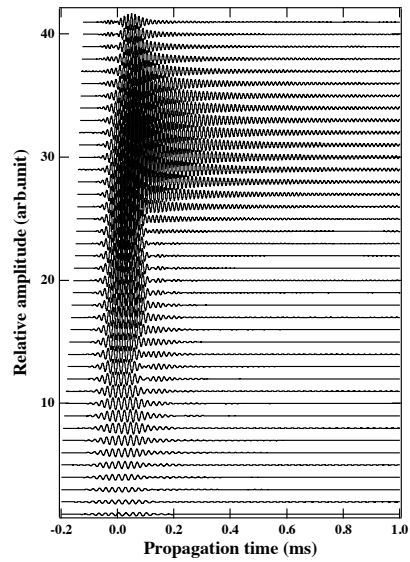
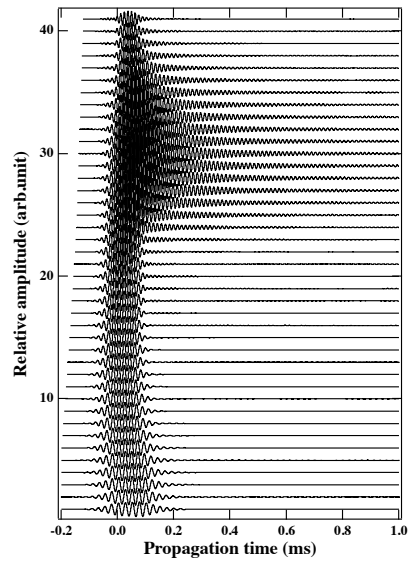
Wall thickness 3.9 mm



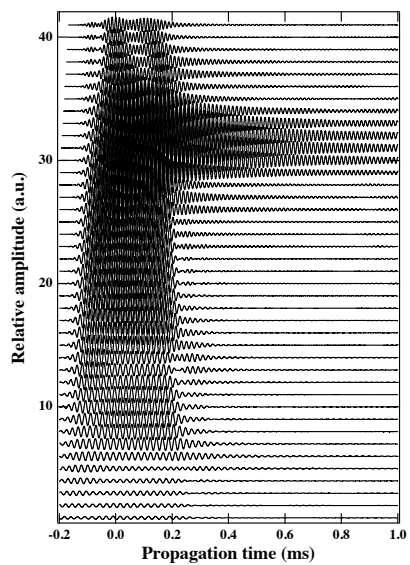
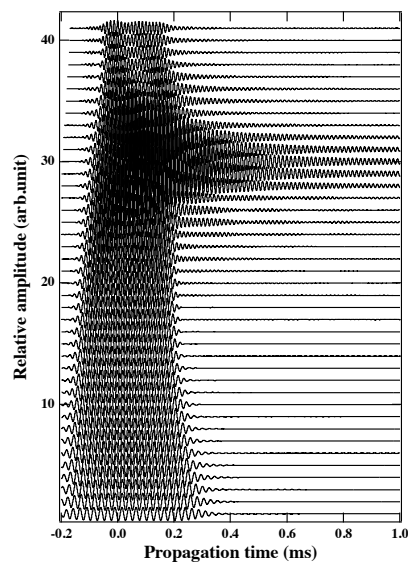
Wall thickness 5.5mm

(b)

Figure 8 Nishino et al

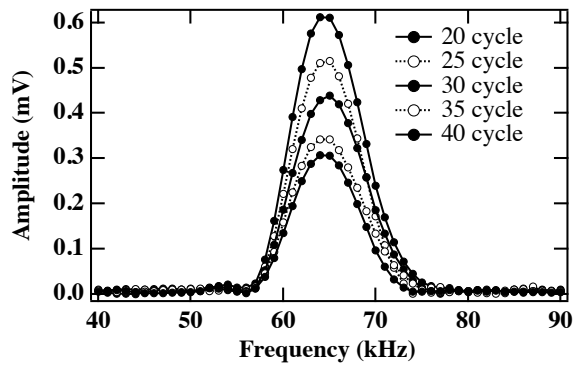


(a)

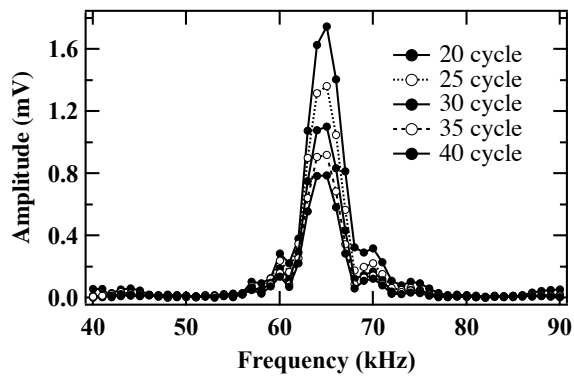


(b)

Figure 9 Nishino et al

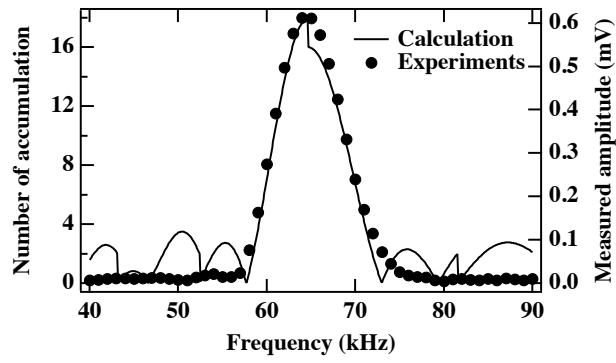


(a)

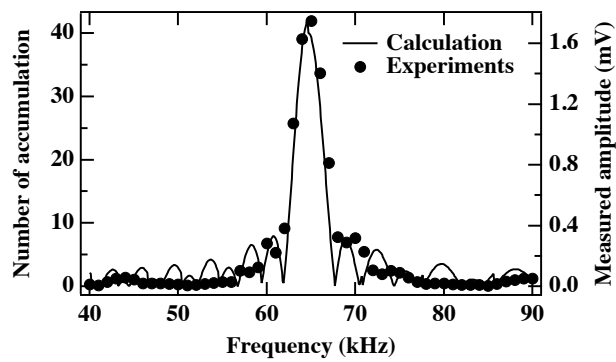


(b)

Figure 10 Nishino et al

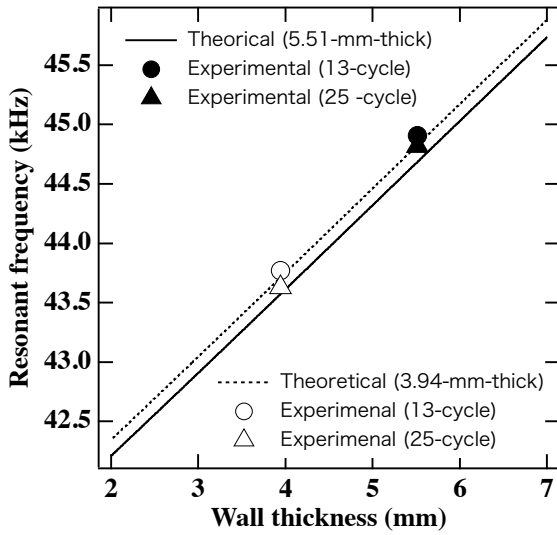


(a)

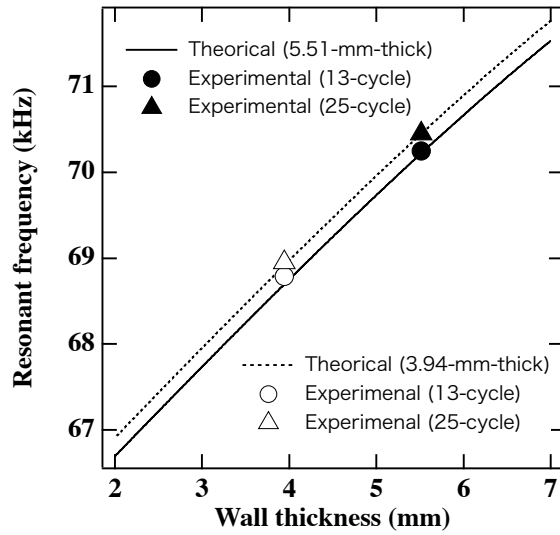


(b)

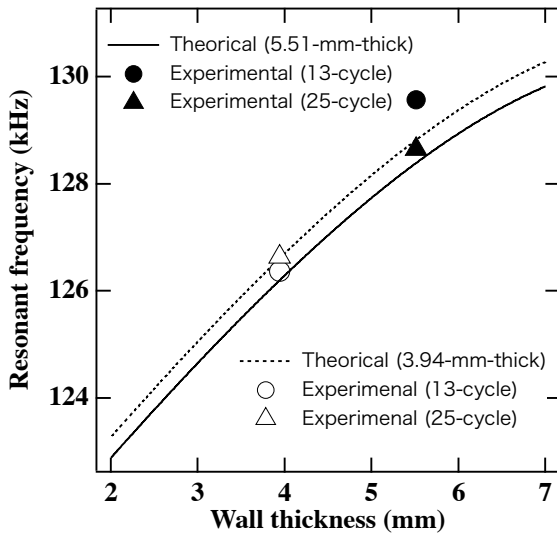
Figure 11 Nishino et al



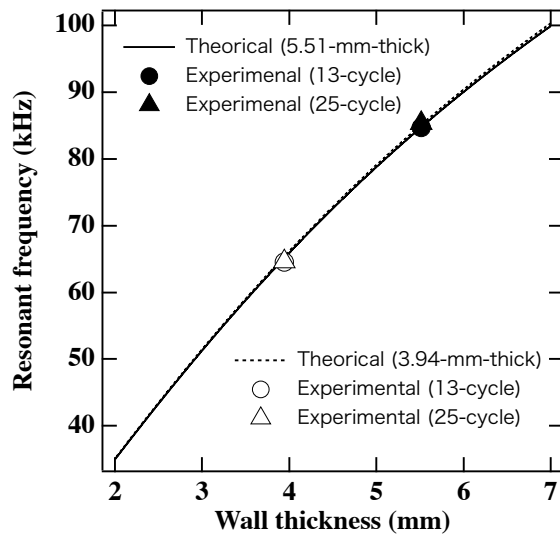
(a)



(b)



(c)



(d)

Figure 12 Nishino et al

Table I. Material properties of aluminum pipes used in the experiments.

	Specimen 1 Nominal thickness: 3.9 mm	Specimen 2 Nominal thickness: 5.5 mm
Outer diameter (mm)	60.52 ± 0.01	60.47 ± 0.03
Wall thickness (mm)	3.94 ± 0.02	5.51 ± 0.06
Shear wave velocity (m/s)	3170 ± 5	3153 ± 7
Longitudinal wave velocity (m/s)	6396 ± 5	6406 ± 7

Table II. Experimental and theoretical resonant frequencies.

		Resonant frequency (kHz)							
		AWN = 1	Error	AWN = 2	Error	AWN = 4	Error	AWN = 8	Error
Specimen 1 (t = 3.94 mm)	Theoretical	43.71	-	68.92	-	126.61	-	65.39	-
	13 cycles	43.77 ± 0.12	(0.1%)	68.79 ± 0.10	(0.2%)	126.37 ± 0.36	(0.2%)	64.57 ± 0.14	(1.2%)
	25 cycles	43.46 ± 0.04	(0.2%)	68.95 ± 0.07	(0.0%)	126.64 ± 0.48	(0.0%)	64.66 ± 0.09	(1.1%)
Specimen 2 (t = 5.51 mm)	Theoretical	44.69	-	70.22	-	128.39	-	84.76	-
	13 cycles	44.91 ± 0.24	(0.5%)	70.25 ± 0.12	(0.0%)	129.57 ± 0.06	(0.9%)	84.75 ± 0.10	(0.0%)
	25 cycles	44.82 ± 0.05	(0.3%)	70.45 ± 0.08	(0.3%)	128.65 ± 0.18	(0.2%)	85.39 ± 0.09	(0.7%)

Table III. Estimated wall thicknesses and their errors to the measured wall thicknesses.

		Wall thickness (mm)							
		AWN = 1	Error	AWN = 2	Error	AWN = 4	Error	AWN = 8	Error
Specimen 1 (t = 3.94 mm)	13 cycles	4.02	(2.0%)	3.81	(3.3%)	3.79	(3.8%)	3.88	(1.5%)
	25 cycles	3.82	(3.1%)	3.97	(0.8%)	3.97	(0.8%)	3.89	(1.3%)
<hr/>									
Specimen 2 (t = 5.51 mm)	13 cycles	5.83	(5.8%)	5.54	(0.5%)	6.67	(21.1%)	5.51	(0.0%)
	25 cycles	5.70	(3.5%)	5.76	(4.5%)	5.74	(4.2%)	5.57	(1.0%)